Mathematical modeling for protein folding devices. Applications to high pressure processing and microfluidic mixers

J. Bello Rivas, J. A. Infante, B. Ivorra, J. López Redondo,
P. Martínez Ortigosa, A. M. Ramos, J. M. Rey, and N. Smith.

Mathematical modeling for protein folding devices. Applications to high pressure processing and microfluidic mixers.

Juan Bello Rivas[1], Juan-Antonio Infante[1], Benjamin Ivorra[1],
Juana López Redondo[2], Pilar Martínez Ortigosa[2],
Angel Manuel Ramos[1], Jose Maria Rey[1], Nadia Smith[1]

[1] Departamento de Matemática Aplicada,
Universidad Complutense de Madrid &
Insituto de Matemática Interdisciplinar,
Plaza de Ciencias, 3, 28040–Madrid, Spain

[2] Dept. de Arquitectura de Computadores y Electrónica,
Universidad de Almeria,
Ctra. Sacramento s/n, La Cañada de San Urbano,
04120 Almería, Spain

June 7, 2010

Abstract

In this paper, we consider two particular devices used for protein folding. The first one is a microfluidic mixer that perform a folding process by mixing a protein solution with a solvent. We are interested in minimizing its mixing time by choosing suitable shape and flow conditions. The second one is related to food processing and we focus on the modeling and simulation of the temperature evolution inside a high pressure food treatment device. Some of the effects of such treatments is to unfold, and thus inactivate, certain enzymes inside the food sample. The behavior and stability of the proposed model is checked by numerical examples. Furthermore, a simplified version of this model is presented and compared in terms of accuracy and computational time.

Keywords: High-Pressure; Protein folding; Mathematical modeling; Global Optimization.

1   Introduction

Proteins are organic compounds made of amino acids that catalyze chemical reactions. Protein folding is a process that consist of a change in the protein structure from a folded state (the protein can perform chemical reaction) to an

unfolded state (the protein becomes inactive). Its range of industrial application is wide: DNA sequencing, drug molecules creation, food treatment, etc.

Protein folding can be performed, for instance, by using photochemical initiation, changes in temperature and/or pressure [20], changes in chemical potential (as in salt or chemical denaturant concentration changes) [7]. All these techniques provide perturbations of a protein conformational equilibrium, necessary to initiate folding.

In this paper we center on two different devices that perform protein folding by using, respectively, concentration and temperature/pressure changes. In the first case, we study a microfluidic mixer used to mix, as fast as possible, a protein solution with a solvent. In particular, we are interested in optimizing the mixer to improve its mixing properties. To do so, we introduce a 2-D model, define the considered parameters and solve the associated optimization problem.

In the second case, we focus on a particular High-Pressure-Temperature treatment device. Its objective is to unfold enzymes (a variety of proteins) inside a food sample in order to prolong its shelf life. In particular, we study a heat-transfer model that predicts the temperature evolution inside the device when the pressure profile is given. As this model is computationally expansive, we also propose and analyze a simplified version.

2 Microfluidic Mixer device

2.1 Device description

Folding experiments based on changes in chemical potential are applicable to a wide range of proteins since most of them unfold reversibly in the presence of chemical denaturants such as urea and guanidine hydrochloride [1].

In this Section, we discuss specific shape and inlet velocities optimization for a microfluidic mixer based on the continuous flow principle originally proposed by Knight et al. [14] and improved and demonstrated by Hertzog et al. [7] (see Figure 1-(a)). We use an optimization approach following Ivorra et al. [6, 12]. The shape of the mixing region was fixed to an intersection at 90 degrees channels, with only variations in the shape intersection.

We are now interested in extending those previous works by solving a more complex optimization problem that involves more geometrical variables (in particular, varying the angle of the intersection channel) and including the inlet velocities.

2.2 Mixer parameterization

The mixer shape considered is the typical three-inlet/single-outlet channel architecture proposed by Knight [14]. Since our model is symmetric (in order to avoid perturbation in the exiting region [12]), we only study half of the mixer [7] (see Figure 1-(a)). Our model is a 2D approximation of the physical system [2] (In practice, the depth of the channels is 10 μm to optimize the fluorescence signal with a confocal system). Experiments show only a 5% deviation from a 3D modeling, which is satisfactory when a 2D model is used as a low-complexity model in optimization [7].
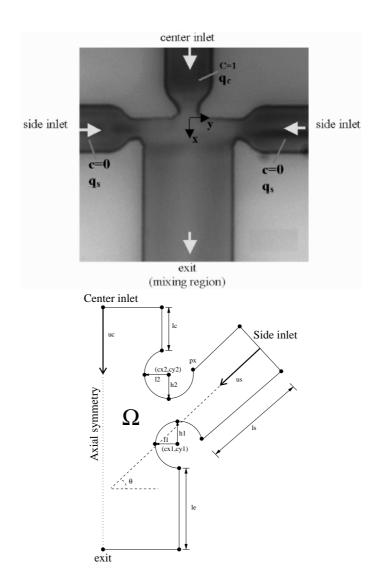
Figure 1: From Top to Bottom: **(a)** Typical fast-micro-mixer geometry. q_s (respectively, q_c) is the side (respectively, center) injection velocity. c is the denaturant concentration. **(b)** Half-Shape parameterization considered for optimization process. The mixers are symmetric respecting to the vertical centerline, so only one symmetric half is used by the model.

We parameterize the mixer shape by using cubic splines (see Figure 1-(b)). The total number of parameters is 15: 2 for the inlet velocities denoted by u_s (side velocity) and u_c (center velocity) (from 0.001 m/s to 1 m/s); 3 for the channel lengths denoted by l_e, l_c and l_s; 1 for the intersection channel angle, denoted by Θ (from 0 degree to 90 degrees); and 9 for the corner intersection between each channel denoted by $(cx1, cy1), l1, h1, (cx2, cy2), l2, h2$ and px.

In addition, we account for the following constraints:

- The lithography step in fabrication limits the shape curvature to a minimum of 1 μm, which implies constraints on the geometrical parameters $\Theta, (cx1, cy1), l1, h1, (cx2, cy2), l2, h2$ and px.

- The width of the side channel nozzles is set to 3 μm and the width of the center channel nozzles to 2 μm to mitigate clogging issues.

- The maximum mixer length is 20μm and its maximum height is 23μm, which implies constraints on the parameters l_e, l_c and l_s.

- The physical properties of buffers and guanidine hydrochloride denaturant used here for protein folding studies have known parameters such as density, viscosity, and diffusivity [6].

- Finally, the maximum side and central flow rate, u_s and u_c, is 1 m s^{-1}. Hence, a typical flow Reynolds number based on micromixer thickness and flow inlet is $Re \sim 150$.

Thus, the corresponding search space of the optimization problem is $\Omega = \prod_{i=1}^{15}[x_i^{\min}, x_i^{\max}]$ where $x_i^{\min}$ (resp. $x_i^{\max}$), the minimum (resp. maximum) value of the ith parameter, are fixed by the previous constraints.

2.3 Modeling

The mixer flow was analyzed using numerical solutions of the full Navier-Stokes fluid flow equations and a Convective Diffusion equation describing concentration fields c of the guanidine hydrochloride denaturant. Only steady configurations have been considered, since we are not interested in the behavior of the device during its transient set up.

These flow simulations were used to explore the guanidine hydrochloride performance on a variety of mixer designs with systematically varied flow and geometric parameters. The model is applied to mixer shape designs described in Figure 1-(b). We approximate the flow at the vertical midplane with two-dimensional flow simulations:

$$\begin{cases} -\nabla \cdot (\eta(\nabla \mathbf{u} + (\nabla \mathbf{u})^\top)) + \rho(\mathbf{u} \cdot \nabla)\mathbf{u} + \nabla p = 0 & \text{in } \Omega, \\ \nabla \cdot \mathbf{u} = 0 & \text{in } \Omega, \\ \nabla \cdot (-D\nabla c + c\mathbf{u}) = 0 & \text{in } \Omega, \end{cases} \quad (1)$$

where Ω is the domain defined by the mixer shape (see Figure 1-(b)), $\mathbf{u}$ is the flow velocity vector (m s^{-1}), p is the pressure field (Pa), c is the concentration distribution, $\rho = 1,013$ kg m^{-3} is the density, $\eta = 110^{-3}$kg m^{-1} s^{-1} is the dynamic viscosity and $D = 2^{-9}$ m^2 s^{-1} is the diffusion coefficient.

Finally, the following boundary conditions are assumed: $\mathbf{u} = 0$ on shape border, $\mathbf{u} = u_s.\text{para}_1$ on side inlets and $\mathbf{u} = u_c.\text{para}_2$ on the center inlet, where

4

para$_1$ and para$_2$ are parabolic functions equals to 0 in the inlet border and 1 in the inlet center; $\mathbf{u} \cdot t = 0$ on the exit; $\mathbf{u} \cdot n = 0$ on the center symmetry line; (t, n) is the local orthonormal reference frame along the boundary; c is prescribed at inlet and normal zero gradient is assumed for all other boundaries; $c = 0$ at side inlet and $c = 1$ at center inlet.

In order to compute a numerical solution, the incompressible Navier-Stokes equation is solved iteratively. We consider Lagrange P2-P1 elements to stabilize the pressure and to satisfy the Ladyzhenskaya, Babouska and Brezzi (LBB) stability condition. More precisely, 2nd-order Lagrange elements model the velocity components while linear elements model the pressure. The convective diffusion equation is solved using a streamline-upwind/Petrov-Galerkin (SUPG) method in order to stabilize the advection. Both of these stabilization techniques prevent numerical oscillations and other instabilities when solving problems with advection-dominated flows, and when using equal-order interpolation functions for velocity and pressure. A Direct Damped Newton method is then used to solve the corresponding linear systems [12].

2.4   Cost Function

The cost function to minimize is the mixing time of the considered Lagrangian fluid particle traveling along the centerline into our fast-micro-mixer with parameters associated to $x_{param} \in \Omega$ and is denoted by $J(x_{\mathrm{param}})$. In this paper, we define mixing time as the time required to change the concentration of a typical protein particle from 90% to 30% of the initial value c_0. Thus, the cost function is given by:

$$J(x_{\mathrm{param}}) = \int_{c_{90}^{x_{\mathrm{param}}}}^{c_{30}^{x_{\mathrm{param}}}} \frac{\mathrm{d}y}{\mathbf{u}^{x_{\mathrm{param}}}(y) \cdot t}, \qquad (2)$$

where $c_{90}^{x_{\mathrm{param}}}$ and $c_{30}^{x_{\mathrm{param}}}$ denote the points along the symmetry line where the concentration is at 90% and 30% of c_0, respectively.

This modeling has been validated by a posteriori prototyping [7].

2.5   Results

In order to solve the optimization problem presented in Section 2.4, we use the *Global Optimization Platform* (*GOP*) software (available at `http://www.mat.ucm.es/momat/software.html`) with a genetic algorithm as the core algorithm and where the initial population is generated using the secant method. A complete description and validation of this algorithm can be found in [10, 11, 12, 13]. Other optimization approaches could have been considered, such as the Universal Evolutionary Global Optimizer (*UEGO*) algorithm which is based on the construction of a greedy solution combined with a local search phase which starts at the constructed solution [21, 22, 23].

The optimization algorithm starts from an initial shape made with smoothed 90 degrees corners parameterized with splines to keep the admissible regularity. The mixing time has been decreased from 8μs to 0.5μs (see Figure 2-a). Optimized shape is presented in Figure 2-b. The number of evaluations is 1000. Each evaluation requires about 40s on a 3.6Ghz Pentium 4 PC computer with 2GB of RAM. Thus the optimization process takes about 11 hours. This optimized
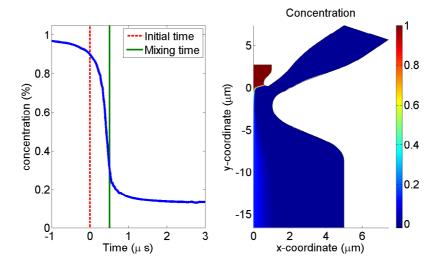
Figure 2: From Left to Right: **(a)** Predicted normalized concentration versus time of the optimized mixer. The initial time (i.e. 0 second), represented by a vertical dashed line, corresponds to the moment when the typical protein particle reaches a concentration of 90%. The final mixing time, represented by a continuous vertical line, corresponds to the moment when the typical protein particle reaches a concentration of 30%. **(b)** Concentration field and shape of the optimized mixer.

mixer is better than the one encountered in previous optimization approaches [12] (without angle and inlet velocities parameters) whose mixing time were 1μs.

3 High-Pressure device

3.1 Device description

Actually, the demand of safe and minimally processed food, prepared for immediate consumption has increased significantly, in order to give service to the needs of restaurants, collective dining rooms as well as to domestic consumption. One of the technologies that can be used for the preparation of these products is High Pressure (HP) Processing, which has become out to be very effective to prolong the shelf life of some foods (cooked ham, juices, guacamole, oysters, etc.) being already a reality at industrial level. These treatments have the great advantage of not being based on the incorporation of additives, which consumers prefer to elude. Furthermore, they allow to avoid treatments with high temperatures (as Pasteurization), which have adverse effects on some nutritional properties of the food, such as its flavor, etc. (see, e.g., [8]).

Some of the effects of the combination of high pressure with thermal treatments on a food sample is to inactivate some undesired enzyme (by unfolding them), prolonging the shelf life of the food. Here we focus on the modeling and simulation of the Pressure-Temperature evolution inside a food sample when such a treatment is applied. Due to the high computational complexity needed

for solving this model (which includes heat and mass transfer and nonconstant thermophysical properties), we also consider and study a simplified version of it. These models could be very important to design suitable industrial equipments and to optimize the processes.

3.2 Modeling

When HP is applied in Food Technology, it is necessary to consider the thermal effects produced by variations of temperature due to the work of compression/expansion in both the food and the pressurizing fluid.

After compression, heat exchange appears between the pressure chamber, the pressure medium and the food sample, giving a time–dependent distribution of temperatures. In the fluid media (the pressurizing fluid and also the food when it is in liquid state), changes in temperatures imply changes in fluid density, leading to free convection during the high pressure process. Therefore, conduction and convection have been considered in the models, taking into account heat and mass transfer (see [3]).

Often, HP experiments are carried out in a cylindrical pressure vessel (typically a hollow steel cylinder) previously filled with the food and the pressure medium. The sample is located in the inner chamber at a temperature that can be either the same or different to the one in the pressure medium and/or the solid domain surrounding it, which may cool or warm the food depending on the user's criteria.

The axial symmetry of the model allows us to consider cylindrical coordinates and the domain given by half a cross section (intersection of the cylinder with a plane containing the axis). Let us consider four bidimensional sub–domains (see Figure 3-(a)):

- Ω_{F}: domain where the sample of food is located.

- Ω_{C}: cap of the sample holder (typically a rubber cap).

- Ω_{P}: domain occupied by the pressurizing medium.

- Ω_{S}: domain of the steel surrounding the above domains.

Our domain in the (r, z)–coordinates is the rectangle $\Omega = [0, L] \times [0, H]$ defined by $\overline{\Omega} = \overline{\Omega_{\mathrm{F}} \cup \Omega_{\mathrm{C}}} \ \overline{\cup \Omega_{\mathrm{P}} \cup \Omega_{\mathrm{S}}}$, where $\{0\} \times (0, H)$ generates the axis of symmetry. In the boundary of Ω, which is denoted by Γ, we distinguish:

- $\Gamma_{\mathrm{r}} \subset \{L\} \times (0, H)$, where the temperature will be known.

- $\Gamma_{\mathrm{up}} = [0, L] \times \{H\}$, where heat transfer with the room where the equipment is located could take place.

- $\Gamma \backslash \{\Gamma_{\mathrm{r}} \cup \Gamma_{\mathrm{up}}\}$, with zero heat flux, either by axial symmetry or by isolation of the equipment.

We denote by Ω^*, Ω_{F}^*, Ω_{C}^*, Ω_{P}^*, Ω_{S}^*, Γ^*, Γ_{r}^* and Γ_{up}^* the domains generated when rotating Ω, Ω_{F}, Ω_{C}, Ω_{P}, Ω_{S}, $\Gamma \backslash (\{0\} \times (0, H))$, Γ_{r} and Γ_{up} along the axis of symmetry (in the 3D space), respectively.

For the mathematical model we will consider a liquid type food. We propose a model considering convection both in the pressurizing medium and the region
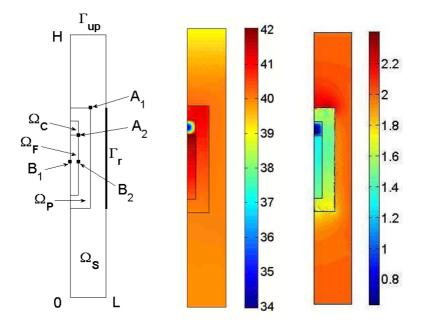
7

Figure 3: From Left to Right: (**a**) Computational domain. (**b**) Temperature distribution (ºC) in the whole domain at $t = 15$ after the considered process. (**c**) Example of temperature average error distribution (ºC) between the full and the perturbed models.

Ω_F. We distinguish two separated velocity fields $\mathbf{u_F}$ and $\mathbf{u_P}$ for the food and the pressurizing fluid, respectively. We point out that the pressure medium and the food are separated by the sample holder and do not mix.

The governing equations are

$$\begin{cases} \rho C_p \dfrac{\partial T}{\partial t} - \nabla \cdot (k\nabla T) + \rho C_p \mathbf{u} \cdot \nabla T = \alpha \dfrac{dP}{dt} T \ \text{ in } \Omega^* \times (0, t_{\mathrm{f}}), \\[2ex] \rho \dfrac{\partial \mathbf{u_F}}{\partial t} - \nabla \cdot \eta (\nabla \mathbf{u_F} + \nabla \mathbf{u_F^t}) + \rho(\mathbf{u_F} \cdot \nabla)\mathbf{u_F} \\[1ex] \qquad = -\nabla p - \nabla \cdot \left(\dfrac{2\eta}{3} (\nabla \cdot \mathbf{u_F})I \right) - \rho \mathbf{g} \ \text{ in } \Omega_{\mathrm{F}}^* \times (0, t_{\mathrm{f}}), \\[2ex] \rho \dfrac{\partial \mathbf{u_P}}{\partial t} - \nabla \cdot \eta (\nabla \mathbf{u_P} + \nabla \mathbf{u_P^t}) + \rho(\mathbf{u_P} \cdot \nabla)\mathbf{u_P} \\[1ex] \qquad = -\nabla p - \nabla \cdot \left(\dfrac{2\eta}{3} (\nabla \cdot \mathbf{u_P})I \right) - \rho \mathbf{g} \ \text{ in } \Omega_{\mathrm{P}}^* \times (0, t_{\mathrm{f}}), \\[2ex] \dfrac{\partial \rho}{\partial t} + \nabla \cdot (\rho \mathbf{u_F}) = 0 \ \text{ in } \Omega_{\mathrm{F}}^* \times (0, t_{\mathrm{f}}), \\[2ex] \dfrac{\partial \rho}{\partial t} + \nabla \cdot (\rho \mathbf{u_P}) = 0 \ \text{ in } \Omega_{\mathrm{P}}^* \times (0, t_{\mathrm{f}}), \end{cases} \quad (3)$$

where P is the pressure (Pa) applied by the equipment, $\mathbf{u} = \mathbf{u_F} + \mathbf{u_P}$ is the total fluid velocity field (ms^{-1}), p is the pressure (Pa) generated by the mass transfer inside the fluid, T is the temperature (K), ρ is the density (kg m^{-3}), C_p is the heat capacity (J kg^{-1} K^{-1}), k is the thermal conductivity (W m^{-1}K^{-1}), t_{f} (s) is the final time, η is the dynamic viscosity (Pa s), $\mathbf{g}$ is the gravity vector (m s^{-2}) and α is the thermal expansion coefficient (K^{-1}) of the food in Ω_{F}^*, of the pressure fluid in Ω_{P}^* and 0 elsewhere.

Right hand term of first equation in (3) results from the following law:

$$\frac{\Delta T}{\Delta P} = \frac{\alpha TV}{MC_p} = \frac{\alpha T}{\rho C_p},$$

where ΔT is the change of temperature due to a change of pressure ΔP, V (m^3) is the volume and M (kg) is the mass.

We also consider the following point, boundary and initial conditions:

$$\begin{cases} k\dfrac{\partial T}{\partial \mathbf{n}} = 0 \ \text{ on } \Gamma^* \backslash (\Gamma_r^* \cup \Gamma_{\mathrm{up}}^*) \times (0, t_{\mathrm{f}}), \\[2ex] k\dfrac{\partial T}{\partial \mathbf{n}} = h(T_{\mathrm{amb}} - T) \ \text{ on } \Gamma_{\mathrm{up}}^* \times (0, t_{\mathrm{f}}), \\[2ex] T = T_{\mathrm{ref}} \ \text{ on } \Gamma_r^* \times (0, t_{\mathrm{f}}), \quad T = T_0 \ \text{ in } \Omega^*, \\[2ex] \mathbf{u_F} = 0 \ \text{ on } \Gamma_{\mathrm{F}}^* \times (0, t_{\mathrm{f}}), \quad \mathbf{u_P} = 0 \ \text{ on } \Gamma_{\mathrm{P}}^* \times (0, t_{\mathrm{f}}), \\[2ex] p = 10^5 \ \text{ in } A_1 \times (0, t_{\mathrm{f}}) \cup A_2 \times (0, t_{\mathrm{f}}), \end{cases} \quad (4)$$

where Γ_{F}^* denotes the boundary of Ω_{F}^*, Γ_{P}^* is the boundary of Ω_{P}^*, A_1, A_2 are corner points of Γ_{P}^* and Γ_{F}^*, respectively (see Figure 3-(a)), $\mathbf{n}$ is the outward normal vector on the boundary of the domain, T_0 us the initial temperature, T_{ref} is the temperature that is kept constant in Γ_r^* (cooling or warming the food sample), T_{amb} is the (constant) temperature at the external environment and h (Wm^{-2}K^{-1}) is the heat transfer coefficient.

3.3 Model sensitivity

In practice, the coefficients used in Equations (3)–(4) are usually approximated using experimental data with a standard deviation inferior to $\pm 5\%$ of the value (see [25]). Furthermore, due to equipment limitations, some experimental discrepancies could occur during the process (for instance, the pressure curve is not strictly respected). In order to study the impact of those errors on the temperature, we perform a sensitivity study on the considered model.

More precisely, we generate $N \in \mathbb{N}$ perturbed models considering the original one, where ρ, C_p, k, α, η, T_0, T_{ref}, P are perturbed uniformly by $\pm 5\%$. Then, we compute the mean temperature error T_{err} as follows:

$$T_{\text{err}} = \frac{1}{N} \sum_{i=1}^{N} ||T - T_i||_{L^2(\Omega \times (0, t_f))}^2, \tag{5}$$

where T is the temperature distribution obtained using the original model and $\{T_i\}_{i=1}^{N}$ are the solutions corresponding to the N perturbed models.

3.4 Simplified model

Due to the high computational complexity needed to solve the "full" model (3)–(4), it may be interesting to consider some simplified versions (called "simplified models"), that are less expansive to evaluate and provide results close enough to the full model. Indeed, simplified models are useful when they are used, for example, during optimization processes needing a lot of model evaluations (see [10, 12]). A description of this methodology can be found in [16].

Thus, we carry out the study of the numerical characteristics of one simplified version of the liquid food model (3)–(4) described previously.

More precisely, we consider a version with constant coefficients (except the density ρ which depends on temperature and pressure in order to keep the effect of the heat transfer by convection in the liquid domains) by setting C_p, k, α and η to their mean value in the range of temperature and pressure considered in the process (other simplifications, as the Boussinesq approximation, could be also considered). This model is denoted by **T–CC**.

In order to evaluate the efficiency of the simplified model, we compute the error made on the temperature (**ET**) considering the simplified model instead of the full one. It is given by

$$\text{ET}(T_{\text{sim}}) = ||T - T_{\text{sim}}||_{L^2(\Omega \times (0, t_f))}^2, \tag{6}$$

where T_{sim} and T are the solution given by the simplified and full models, respectively.

3.5 Numerical tests

For the numerical experiments we have used the dimensions of the pilot unit (ACB GEC Alsthom, Nantes, France) that was used in [19]. Therefore, the 2D cylindrical domain has a radius of $L = 0.09$ m and a height of $H = 0.654$ m (see Figure 3-(a)).

We consider a representative example of sample food: a liquid type food with a small filing ratio. The dimensions and location of the sample is exactly the same as studied in [19] for solid type foods.

We present numerical tests computed in cylindrical coordinates using an iterative solver. We have considered a finite element approach for solving the model. More precisely, velocity and pressure spatial discretization is based on P2–P1 Lagrange Finite Elements satisfying the Ladyzhenskaya, Babuska and Brezzi (LBB) stability condition. The convective diffusion equation is solved using a suitable direct method (UMFPACK: Unsymmetric MultiFrontal method for sparse linear systems) combined with a stabilization technique (GLS: Galerkin Least Squares, see [26]).

The physical parameters of the pressurizing medium are supposed to be equal to those of the water and depending on temperature and pressure. For the liquid food sample, water physical parameters are considered too. In this case, ρ, C_p and k parameters are computed through a *shifting approach* (see [18]) from atmospheric pressure, and using a suitable linear interpolation for other values of pressure. For the parameter α we use the expression described in [17]. Finally, dynamic viscosity η is obtained also by interpolation of data obtained using [15].

For general cases where the thermophysical properties of a particular food are not known, mathematical tools for inverse problems may be needed for their identification. For example, in [5] the authors discuss how to identify the heat transfer coefficient for a particular prototype. Identification of coefficients depending on temperature is considered, in a rigorous mathematical way in [4] for a general abstract case.

The environmental temperature, the reference temperature and the heat transfer coefficient used in the test are $T_{\mathrm{amb}} = 19.3$ °C, $T_{\mathrm{ref}} = 40$ °C and $h = 28$ W m^{-2} K^{-1}, respectively. Initial temperature in the sample is chosen equal to 22 °C. Thermophysical properties of the steel and the rubber cap of the sample holder were considered to be constant ($\rho = 7833$ kg m^{-3}, $C_p = 465$ J kg^{-1} K^{-1} and $k = 55$ W m^{-1} K^{-1} for steel and $\rho = 1110$ kg m^{-3}, $C_p = 1884$ J kg^{-1} K^{-1} and $k = 0.173$ W m^{-1} K^{-1} for rubber).

We have performed several numerical experiments simulating the temperature evolution. For this sake, we consider a high pressure process as follows: for initial temperature $T_0 = 40$ °C in Ω_{S}, and $T_0 = 22$ °C in $\Omega \backslash \Omega_{\mathrm{S}}$, a constant pressure increase in the first 305 seconds until reaching 600 MPa is considered. Therefore, the derivative of pressure in the internal heat generation is $\frac{\mathrm{d}P}{\mathrm{d}t}(t) = \frac{600}{305} 10^6$ Pa s^{-1}, when $0 < t \leq 305$, and 0 Pa s^{-1}, when $t > 305$.

3.5.1 Full model analysis

Figure 3-(b) shows the temperature distribution under the considered high pressure process at time $t = 15$ min. It illustrates how the model captures the nonhomogeneous temperature distribution in the domain.

Figure 4-(a) plots the evolution of the temperature at two points: the first one, B_1, is located at the center of the sample (at the symmetry axis) and the second one, B_2, at the surface of the sample, located at the same height than B_1 (see Figure 4-(b)). Evolution of sample mean temperature is also plotted.

Therefore, the model and the numerical approximation of its solution is consistent with what is physically expected.

As already remarked in [19] for solid type foods, these results show that for liquid foods it can be also interesting to use an initial temperature for the food smaller than T_{ref} in order to anticipate the temperature increase that
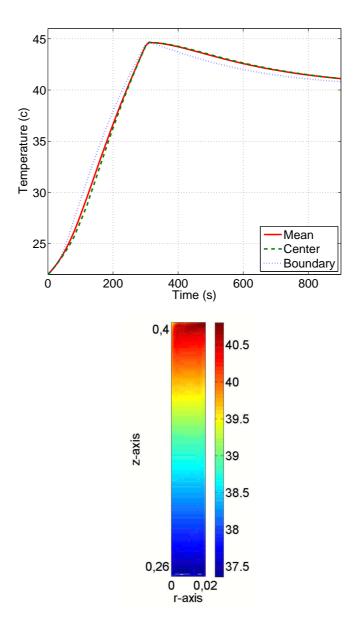
Figure 4: From Top to Bottom: **(a)** Evolution of the sample's mean temperature (—), temperature in the center point B_1 (- -) and in the boundary point B_2 (...) of the sample during the process. **(b)** Time–averaged temperature distribution (°C) during 15 min in the food sample after the considered process.

12

results from compression, which allows to get a more uniform process avoiding big temperature gradients inside the food and temperatures much higher than T_{ref} (remember that one of the goals of high–pressure technology is to process food without using high temperatures, which degrade some of the foods main qualities).

3.5.2 Model sensitivity analysis

According to Section 3.3, in order to evaluate the sensitivity of our model, we have generated $N = 10$ perturbed versions of the model. The mean temperature error defined in (5) satisfies $T_{\text{err}} \leq 2$ C. This represents $\pm 8\%$ of the range of temperature $[21\ ^{\circ}\text{C}, 47\ ^{\circ}\text{C}]$ reached during the processes.

Furthermore, as we can observe in Figure 3-(c), which represents an example of the distribution of the error in the whole equipment, the average error committed in the food sample, close to 1.2 $^{\circ}$C ($\pm 5\%$), is less important than the error committed in the other parts of the device.

3.5.3 Simplified model analysis

The **T–CC** model produces an error of $ET(T_{\text{T-CC}})$=0.15 $^{\circ}$C ($\pm 0.6\%$). This simplified model gives a good alternative to the full one for possible optimization procedures as its computational time is 7500s against 35000s of the full model, when considering a 3.6Ghz Pentium 4 PC computer with 2GB of RAM.

4 Conclusions

The two mathematical models described in this paper provide a useful tool to evaluate and optimize protein folding process devices based on either thermal and pressure change or concentration change. Those model should be coupled to other kind of model in order to study their effect on the considered protein. For instance, we can combine the model presented in Section 3 with a first order kinetic model to evaluate the impact of HP-T treatment on the enzyme activity in a food sample. A full description of this coupling can be found in [9].

Acknowledgments

References

[1] C.K. Chan, Y. Hu, S. Takahashi, D.L. Rousseau, and W.A. Eaton, Submillisecond protein folding kinetics studied by ultrarapid mixing, *Proceedings of the National Academy of Sciences of the USA*, **94**, 1779-1784 (1997).

[2] N. Darnton, O. Bakajin, and R. Huang, B. North, J. Tegenfeldt, E. Cox, J. Sturn and R. H. Austin, Condensed Matter, *Journal of Physics*, **13**, 4891-4902 (2001).

[3] A. Delgado, C. Rauh, W. Kowalczyk and A. Baars, *Review of modeling and simulation of high pressure treatment of materials of biological origin*, Trends in Food Science & Technology **19(6)**, 329–336 (2008).

[4] A. Fraguela, J.A. Infante, A.M. Ramos and J.M. Rey, *Identification of a heat transfer coefficient when it is a function depending on temperature*, WSEAS Trans. Math. **7(4)**, 160–172 (2008).

[5] B. Guignon, A.M. Ramos, J.A. Infante, J.M. Díaz and P.D. Sanz, *Determining thermal parameters in the cooling of a small-scale high pressure freezing vessel*, International Journal of Refrigeration, **29**, 1152–1159 (2006).

[6] D.E. Hertzog, B. Ivorra, B. Mohammadi, O. Bakajin, J.G. Santiago, Optimization of a Microfluidic Mixer for Studying Protein Folding Kinetics, *Analytical chemistry*, **78(13)**, 4299–4306 (2006).

[7] D.E. Hertzog, X. Michalet, M. Jager, X. Kong, J.G. Santiago, S. Weiss, and O. Bakajin, Femtomole Mixer for Microsecond Kinetic Studies of Protein Folding, *Analytical Chemistry*, **75 (24)**, 7169-7178 (2004).

[8] I. Indrawati, A.M. van Loey, C. Smout and M.E. Hendrickx, *High hydrostatic pressure technology in food preservation*. In *Food preservation techniques*, Woodhead Publ. Ltd., Cambridge, 428–448 (2003).

[9] J. A. Infante, B. Ivorra, A.M. Ramos del Olmo and J. M. Rey. On the Modeling and Simulation of High Pressure Processes and Inactivation of Enzymes in Food Engineering. Mathematical Models and Methods in Applied Sciences, **19(12)**, 2203–2229 (2009).

[10] B. Ivorra, B. Mohammadi, L. Dumas, O. Durand and P. Redont, *Semi–deterministic vs. genetic algorithms for global optimization of multichannel optical filters*, International Journal of Computational Science for Engineering, **2(3)**, 170–178 (2006).

[11] B. Ivorra, B. Mohammadi, and A.M. Ramos, Optimization strategies in credit portfolio management. *Journal Of Global Optimization*, **43(2)**:415–427 (2009).

[12] B. Ivorra, B. Mohammadi, D.E. Santiago and J.G. Hertzog, *Semi–deterministic and genetic algorithms for global optimization of microfluidic protein folding devices*, International Journal of Numerical Method in Engineering **66(2)**, 319–333 (2006).

[13] B. Ivorra, A.M. Ramos, and B. Mohammadi (2007) Semideterministic global optimization method: Application to a control problem of the burgers equation. *Journal of Optimization Theory and Applications*, 135(3):549–561.

[14] J.B. Knight, A. Vishwanath, J.P. Brody, and R. H. Austin, Hydrodynamic Focusing on a Silicon Chip: Mixing Nanoliters in Microseconds, *Physical Review Letters* , **80**, 3863-3866 (1998).

[15] E.W. Lemmon, M.O. McLinden and D.G. Friend, *Thermophysical properties of fluid systems.* In Linstron P.J. & Mallard W.G. (Eds.), *NIST Chemistry Web Book. NIST Standard Reference Database*, **69** (June 2005). National Institute of Standards and Technology. Gaitherburg MD.

[16] B. Mohammadi, J. Santiago and J. Molho, *Incomplete sensitivities in the design of minimal dispersion fluidic channels*, Comput. Methods Appl. Mech. Engrg. **192**, 4131–4145 (2003).

[17] L. Otero, A.D. Molina–García and P.D. Sanz, *Some interrelated thermophysical properties of liquid water and ice I. A user–friendly modeling review for food high–pressure processing*, Critical Reviews in Food Science and Nutrition **42(4)**, 339–352 (2002).

[18] L. Otero, A. Ousegui, B. Guignon, A. Le Bail and P.D. Sanz, *Evaluation of the thermophysical properties of tylose gel under pressure in the phase change domain*, Food Hydrocolloids **20**, 449-460 (2006).

[19] L. Otero, Á.M. Ramos, C. de Elvira and P.D. Sanz, *A Model to Design High–Pressure Processes Towards an Uniform Temperature Distribution*, J. Food Eng. **78**, 1463–1470 (2007).

[20] K. M. Pryse, T.G. Bruckman, B.W. Maxfield, and E.L. Elson, Kinetics and mechanism of the folding of cytochrome c, *Biochemistry*, **31(22)**, 5127-5136, (1992).

[21] J.L. Redondo, J. Fernández, I. García, and P.M. Ortigosa. A robust and efficient global optimization algorithm for planar competitive location problems. *Annals of Operations Research*, **167**, 87-105 (2009).

[22] J.L. Redondo, J. Fernández, I. García, and P.M. Ortigosa. Solving the Multiple Competitive Location and Design Problem on the Plane. *Evolutionary Computation*, **17(1)**, 21-53 (2009).

[23] J.L. Redondo, J. Fernández, I. García, and P.M. Ortigosa. Parallel algorithms for continuous competitive location problems. *Optimization Methods & Software*, **23(5)**, 779-791 (2008).

[24] H. Roder, Stepwise helix formation and chain compaction during protein folding, *Proceedings of the National Academy of Sciences of the USA*, **101**, 1793-1794 (2004).

[25] A. Tansakul and P. Chaisawang, *Thermophysical properties of coconut milk*, Journal of Food Engineering **73(3)**, 273–280 (2006).

[26] S. Turek, *Efficient Solvers for Incompressible Flow Problems: An Algorithmic Approach in View of Computational Aspects.* In LNCSE **6**, Springer–Verlag (1999).

1. DESIGN OF CODE DIVISION MULTIPLE ACCESS FILTERS USING GLOBAL OPTIMIZATION TECHNIQUES, B. Ivorra, B. Mohammadi, and A. M.Ramos

2. DYNAMICS IN DUMBBELL DOMAINS II. THE LIMITING PROBLEM, J.M. Arrieta, A. N. Carvalho and G. Lozada-Cruz

3. DYNAMICS IN DUMBBELL DOMAINS III. CONTINUITY OF ATTRACTORS , J. M. Arrieta, A. N. Carvalho and G. Lozada-Cruz

4. GEOMETRIC VERSUS SPECTRAL CONVERGENCE FOR THE NEUMANN LAPLACIAN UNDER EXTERIOR PERTURBATIONS OF THE DOMAIN , J. M. Arrieta and D. Krejcirik

5. ON THE MODELLING AND SIMULATION OF HIGH PRESSURE PROCESSES AND INACTIVATION OF ENZYMES IN FOOD ENGINEERING, J.A. Infante, B. Ivorra, Á.M. Ramos and J.M. Rey

6. CHARACTERIZATION OF THE MARTIAN SURFACE LAYER, G.Martínez, F. Valero, L. Vazquez.

7. CHARACTERIZATION OF THE MARTIAN CONVECTIVE BOUNDARY LAYER, G.Martínez, F. Valero, L. Vazquez.

8. INFINITE RESONANT SOLUTIONS AND TURNING POINTS IN A PROBLEM WITH UNBOUNDED BIFURCATION, J.M. Arrieta, R.Pardo, A.Rodríguez—Bernal

9. CASCADES OF HOPF BIFURCATIONS FROM BOUNDARY DELAY, J.M. Arrieta, N. Cónsul, S. Oliva

10. QUENCHING PHENOMENA FOR A NON-LOCAL DIFFUSION EQUATION WITH A SINGULAR ABSORPTION, R. Ferreira

11. WELL-POSEDNESS OF THE EINSTEIN–EULER SYSTEM IN ASYMPTOTICALLY FLAT SPACETIMES: THE CONSTRAINT EQUATIONS, U. Brauer and L. Karp

12. WELL-POSEDNESS OF THE EINSTEIN–EULER SYSTEM IN ASYMPTOTICALLY FLAT SPACETIMES: THE EVOLUTION EQUATIONS, U. Brauer and L. Karp

13. EXTREMAL EQUILIBRIA FOR MONOTONE SEMIGROUPS IN ORDERED SPACES WITH APPLICATIONS TO EVOLUTIONARY EQUATIONS, J. W. Cholewa and A. Rodriguez-Bernal

14. ASYMPTOTIC BEHAVIOUR OF A PARABOLIC PROBLEM WITH TERMS CONCENTRATED IN THE BOUNDARY, A. Jiménez-Casas and A. Rodriguez-Bernal

15. ASYMPTOTIC BEHAVIOR OF REACTION DIFFUSION EQUATIONS IN WEIGHTED SOBOLEV SPACES, J.M. Arrieta, N. Moya and A. Rodriguez-Bernal

1. CONTINUITY OF DYNAMICAL STRUCTURES FOR NON-AUTONOMOUS EVOLUTION EQUATIONS UNDER SINGULAR PERTURBATIONS, J. Arrieta, A. N. Carvalho, J. Langa and A. Rodríguez-Bernal.

2. ON THE LONG TIME BEHAVIOUR OF NON-AUTONOMOUS LOTKA-VOLTERRA MODELS WITH DIFFUSION VIA THE SUB-SUPER TRA JECTORY METHOD, J.A. Langa, A. Rodríguez-Bernal and A. Suárez.

3. MODELLING AND SIMULATION OF A POLLUTED WATER PUMPING PROCESS, C. Alavani, R. Glowinski, S. Gomez, B.Ivorra, P. Joshi and A. M. Ramos.

4. EXPANDING THE ASYMPTOTIC EXPLOSIVE BOUNDARY BEHAVIOR OF LARGE SOLUTIONS TO A SEMILINEAR ELLIPTIC EQUATION, S. Alarcón, G. Díaz, R. Letelier and J. M. Rey.

5. A SINGULAR PERTURBATION IN A LINEAR PARABOLIC EQUATION WITH TERMS CONCENTRATING ON THE BOUNDARY, A. Rodríguez-Bernal.

6. ISOTHERMALISATION FOR A NON-LOCAL HEAT EQUATION, E. Chasseigne and R. Ferreira.

7. HOMOGENIZATION IN A THIN DOMAIN WITH AN OSCILLATORY BOUNDARY, J. M. Arrieta and M. C. Pereira

8. VERY RAPIDLY VARYING BOUNDARIES IN EQUATIONS WITH NONLINEAR BOUNDARY CONDITIONS. THE CASE OF A NON UNIFORMLY LIPSCHITZ DEFORMATION, J.M. Arrieta and S. Bruschi

9. PERTURBATION OF ANALYTIC SEMIGROUPS IN SCALES OF BANACH SPACES AND APPLICATIONS TO PARABOLIC EQUATIONS WITH LOW REGULARITY DATA, A. Rodríguez-Bernal

10. IDENTIFICATION OF A PRESSURE DEPENDENT HEAT TRANSFER COEFFICIENT, A. Fraguela, J. A. Infante, Á. M. Ramos and J. M. Rey.

11. MATHEMATICAL MODELING FOR PROTEIN FOLDING DEVICES. APPLICATIONS TO HIGH PRESSURE PROCESSING AND MICROFLUIDIC MIXERS, J. Bello Rivas, J. A. Infante, B. Ivorra, J. López Redondo, P. Martínez Ortigosa, A. M. Ramos, J. M. Rey, and N. Smith